

Quantal molecular description and universal aspects of the spectra of bosons and fermions in the lowest Landau level

Constantine Yannouleas* and Uzi Landman†

School of Physics, Georgia Institute of Technology, Atlanta, Georgia 30332-0430, USA

(Received 3 December 2008; published 17 February 2010)

Through the introduction of a class of trial wave functions portraying combined rotations and vibrations of molecules formed through particle localization in concentric polygonal rings, a correlated basis is constructed that spans the translationally invariant part of the lowest-Landau-level (LLL) spectra. These trial functions, referred to as rovibrational molecular (RVM) functions, generalize our previous work that focused exclusively on electronic cusp states, describing them as pure vibrationless rotations. From a computational viewpoint, the RVM correlated basis enables controlled and systematic improvements of the original strongly correlated variational wave function. Conceptually, it provides the basis for the development of a quantal molecular description for the full LLL spectra. This quantal molecular description is universal, being valid for both bosons and fermions, for both the yrast and excited states of the LLL spectra, and for both low and high angular momenta. Furthermore, it follows that all other translationally invariant trial functions (e.g., the Jastrow-Laughlin, compact composite-fermion, or Moore-Read functions) are reducible to a description in terms of an excited rotating and vibrating quantal molecule.

DOI: [10.1103/PhysRevA.81.023609](https://doi.org/10.1103/PhysRevA.81.023609)

PACS number(s): 03.75.Hh, 73.43.-f, 03.75.Lm, 73.21.La

I. INTRODUCTION

A. Motivation

Following the discovery [1] of the fractional quantum Hall effect (FQHE) in two-dimensional (2D) semiconductor heterostructures under high magnetic fields (B) in the 1980's, the description of strongly correlated electrons in the lowest Landau level (LLL) developed into a major branch of theoretical condensed matter physics [2–19]. Early on, it was realized that the essential many-body physics in the LLL can be captured through trial wave functions. Prominent examples are the Jastrow-type Laughlin (JL) [2], composite fermion (CF) [6], and Moore-Read (MR) [7] Pfaffian functions, representing quantum-liquid states [2]. In the last ten years, the field of semiconductor quantum dots [15] helped to focus attention on finite systems with a small number (N) of electrons. Theoretical investigations of such finite systems led to the introduction of “crystalline”-type LLL trial functions referred to as rotating electron molecules [12,15] (REM's). In particular in their intrinsic frame of reference, the REM's describe electrons localized at the apexes of concentric polygonal-ring configurations (n_1, n_2, \dots, n_r) , where $\sum_{q=1}^r n_q = N$ and r is the number of concentric rings.

More recently, the emerging field of graphene quantum dots [20,21] and the burgeoning field of rapidly rotating trapped ultracold neutral gases [22–34] have generated significant interest pertaining to strongly correlated states in the LLL. Furthermore, it is anticipated that small (and/or mesoscopic) assemblies of ultracold bosonic atoms will become technically available in the near future [32–35] and that they will provide an excellent vehicle [27,28,31–35] for experimentally reaching exotic phases and for testing the rich variety of proposed LLL trial wave functions.

Despite the rich literature and unabated theoretical interest, a unifying physical (as well as mathematical) description of the full LLL spectra (including both yrast [36] and all excited states), however, is still missing. In this article, a universal theory for the LLL spectra of a finite number of particles valid for both statistics (i.e., for both bosons and fermions) is introduced. The LLL spectra are shown to be associated with *fully quantal* [37] and strongly correlated rovibrational molecular (RVM) states, that is, with (analytic) trial functions describing vibrational excitations relative to the set of the special yrast states known as cusp states.

The cusp states exhibit enhanced stability and magic angular momenta and as such they have attracted considerable attention. However, the cusp states represent only a small fraction of the LLL spectrum. The molecular trial functions associated with them are purely rotational (i.e., vibrationless) and were introduced for the case of electrons in Ref. [12] as REM's. The corresponding purely rotational bosonic *analytic* trial functions for cusp states [called RBM's] are introduced in this article; see Sec. II A. More importantly, this article shows that the quantal molecular description can be extended to all other LLL states (beyond the special cusp states) by introducing (see Sec. II D) analytic expressions for trial functions representing *rovibrational excitations* of both REM's and RBM's. These rovibrational trial functions include the REM or RBM expressions as a special case and they will be referred to in general as RVM trial functions.

It is remarkable that the numerical results of the present theory were found in all tested cases to be amenable (if so desired) to an agreement within machine precision with exact-diagonalization (EXD) results, including energies, wave functions, and overlaps. This numerical behavior points toward a deeper mathematical finding, that is, that the RVM trial functions for both statistics provide a *complete* and *correlated* basis that spans the translationally invariant (TI) subspace [5] of the LLL spectrum. An uncorrelated basis, without physical meaning, built out of products of elementary

*Constantine.Yannouleas@physics.gatech.edu

†Uzi.Landman@physics.gatech.edu

symmetric polynomials is also known to span the (bosonic) TI subspace [38].

For the sake of clarity, we comment here on the use of the terms “correlated functions” and/or “correlated basis.” Indeed, the exact many-body eigenstates are customarily called correlated when interactions play a dominant role. Consequently, a basis is called correlated when its members incorporate or anticipate effects of the strong two-body interaction a priori (before the explicit use of the two-body interaction in an exact diagonalization). In this respect, Jastrow-type basis wave functions (e.g., the Feenberg–Clark method of correlated-basis functions [39–41] and/or the composite-fermion basis [18,19,42,43]) are described as correlated since the Jastrow factors incorporate the effect of a strong two-body repulsion in keeping the interacting particles apart on the average. Our RVM basis is referred to as correlated since, in addition to keeping the interacting particles away from each other, the RVM functions incorporate the strong-two-body-repulsion effect of particle localization in concentric polygonal rings and formation of Wigner molecules; this localization effect was repeatedly demonstrated via EXD calculations in the past decade (see, e.g., the review in Ref. [15] and references therein). In this spirit, we describe the basis of elementary symmetric polynomials as “uncorrelated,” since the elementary symmetric polynomials do not incorporate or anticipate this dominant effect of a strong two-body repulsion (i.e., that of keeping the interacting particles apart).

We are unaware of any other strongly correlated functions that span the TI subspace. Indeed, although the JL function (used for describing yrast states) is translationally invariant, its quasihole and quasielectron excitations are not [5]. Similarly, the compact CF trial functions are translationally invariant [30], but the CF excitations that are needed to complete the CF basis are not [18,19,42,44]. The shortcoming of the aforementioned well-known correlated LLL theories to satisfy fundamental symmetries of the many-body Hamiltonian represents an unsatisfactory state of affairs and the present article provides a remedy to this effect. In this context, we note that, although the MR functions [7] are also translationally invariant, they address only certain specific LLL states and they do not form a basis spanning the TI subspace.

Our introduction of a correlated basis that spans the TI subspace is of importance in the following two ways: (1) From a practical (and calculational) viewpoint, one can perform controlled and systematic stepwise improvements of the original strongly correlated variational wave function, for example, the pure REM or RBM. (For detailed illustrative examples of the rapid-convergence properties of the RVM basis, see the Appendix.) This calculational viewpoint was also the motivation behind the introduction of other correlated bases in many-body physics; (see, e.g., the treatment of quantum liquids and nuclear matter in Refs. [39–41] and the composite-fermion correlated basis in Refs. [18,19,42,43]). (2) Conceptually, it guarantees that the properties of the RVM functions and, in particular, the molecular point-group symmetries are irrevocably incorporated in the properties of the exact LLL wave functions. Furthermore, it follows that all other translationally invariant trial functions (e.g., the JL, compact CF, or MR functions), are reducible to a description in terms of an excited rotating and vibrating quantal molecule.

Specific examples of the reducibility of the JL and MR states to the molecular description introduced in this article are provided in Secs. III C and III D. This is a surprising result, since these Jastrow-based trial functions are widely described in the previous literature as being liquid-like in an essential way.

B. Characteristic properties of the lowest-Landau-level spectra

For completeness and clarity in the presentation, we briefly provide in this section a graphical illustration of some of the main characteristics of the LLL spectra, calculated via the exact-diagonalization approach.

First we describe here the special form [11,15,30] of the many-body Hamiltonian used for calculating the *global* ground state of a finite number N of electrons at a given magnetic field B . This special form takes advantage of the simplifications at the limit of large B , that is, when the relevant Hilbert space can be restricted to the LLL, given that $\hbar\omega_0 \ll \hbar\omega_c/2$; the frequency ω_0 specifies the external harmonic confinement and $\omega_c = eB/(mc)$ is the cyclotron frequency. Then the many-body Hamiltonian reduces to

$$H_{\text{LLL}}^{\text{e,global}} = N \frac{\hbar\omega_c}{2} + \hbar \left(\sqrt{\omega_0^2 + \omega_c^2/4} - \omega_c/2 \right) L + \sum_{i<j}^N \frac{e^2}{\kappa|z_i - z_j|}, \quad (1)$$

where $L = \sum_{i=1}^N l_i$ is the total angular momentum and $z = x + iy$.

In the case of N rapidly rotating bosons (with ω_0 specifying the external confinement of the 2D harmonic trap and Ω denoting the rotational frequency), the corresponding Hamiltonian [24,25,29,45] (in the limit $\Omega/\omega_0 \rightarrow 1$) is written as [46]

$$H_{\text{LLL}}^{\text{b,global}} = N\hbar\omega_0 + \hbar(\omega_0 - \Omega)L + \sum_{i<j}^N g\delta(z_i - z_j). \quad (2)$$

Since we will consider many-body energy eigenstates that are eigenstates of the total angular momentum as well, it follows that only the interaction terms are nontrivial in both Hamiltonians (1) and (2). As a result, we will henceforth follow the practice of focusing on the simpler interaction-only LLL Hamiltonian

$$H_{\text{LLL}} = \sum_{i<j}^N v(z_i - z_j), \quad (3)$$

where $v(z_i - z_j)$ denotes the two-body interaction (Coulomb for electrons and repulsive contact potential for bosons). The “ground states” of the Hamiltonian in Eq. (3) coincide with the “yrast” band [36].

We remind the reader that the EXD method is based on the fact that the full LLL Hilbert space at a given total angular momentum L is spanned by the set of all possible uncorrelated permanents (for bosons) or Slater determinants (for electrons) made out from the Darwin-Fock zero-node single-particle

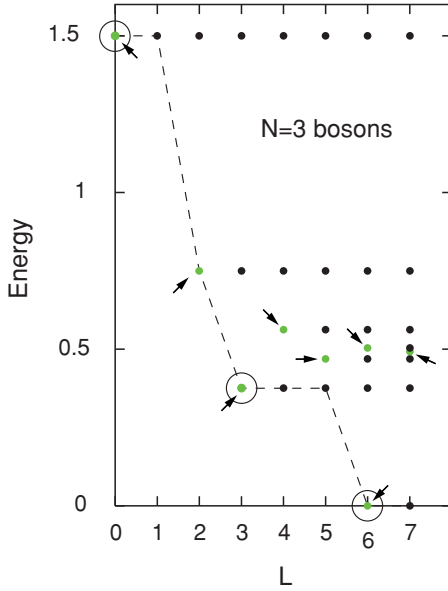


FIG. 1. (Color online) LLL spectra for $N = 3$ scalar bosons calculated using exact diagonalization. Only the Hamiltonian term containing the two-body repulsive contact interaction $g\delta(z_i - z_j)$ [see Eq. (3)] was considered in the exact diagonalization. The gray solid dots (marked by arrows; green online) denote the translationally invariant states. The dark solid dots are the spurious states (see text). The dashed line denotes the yrast band, while the cusp states are marked by a circle. Energies in units of $g/(\pi\Lambda^2)$. The number of translationally invariant states is much smaller than the total number of LLL states.

levels (referred to also as orbitals)

$$\psi_{l_i}(z) = \frac{z^{l_i}}{\sqrt{\pi l_i!}} \exp(-zz^*/2), \quad (4)$$

with $l_i \geq 0$. The position variable z is given in units of $\Lambda = \sqrt{\hbar/(m\omega_0)}$ in the case of a rotating harmonic trap (with lateral confinement frequency ω_0) or $l_B\sqrt{2}$ in the case of an applied magnetic field B , with $l_B = \sqrt{\hbar/(m\omega_c)}$ being the magnetic length and ω_c the cyclotron frequency [46]. (For details concerning the EXD method, see, e.g., Refs. [15,29].) In the following, we use the convention that an uncorrelated state is described by a single permanent (or Slater determinant) made out from the orbitals in Eq. (4), which are characterized by good single-particle angular momenta l_i .

A small part (sufficient for our purposes here) of the EXD LLL spectra (as a function of L) are plotted in Fig. 1 for $N = 3$ scalar bosons and in Fig. 2 for $N = 4$ spin-polarized electrons. As is usually done in the LLL, the one-body terms of the Hamiltonian (i.e., confining potential and kinetic-energy) were omitted [11,15,30] and the exact diagonalization involved only the two-body interaction [see Eq. (3)].

In Figs. 1 and 2, the yrast bands [36] are denoted by a dashed line. Along the yrast bands there appear special cusp states denoted by a circle. The cusp states are important because they exhibit enhanced stability when the one-body terms of the Hamiltonian (i.e., external confinement and kinetic energy) are added [see Eqs. (1) and (2)] and thus they determine [47] the *global ground states* [11,15,24,29,48] as a function of the applied magnetic field B or the rotational frequency Ω

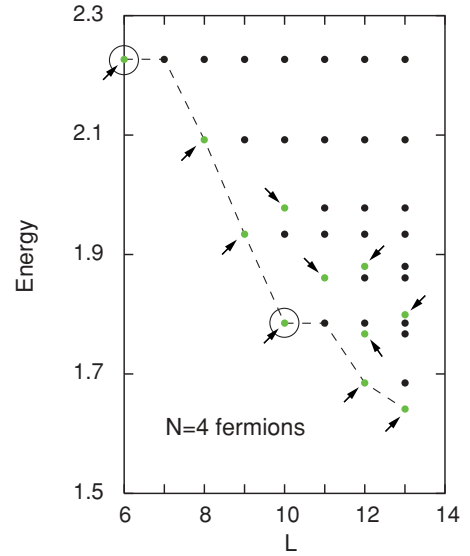


FIG. 2. (Color online) LLL spectra for $N = 4$ spin-polarized electrons calculated using exact diagonalization. Only the Hamiltonian term containing the two-body Coulomb interaction, $e^2/(\kappa|z_i - z_j|)$, [see Eq. (3)] was considered in the exact diagonalization. The gray solid dots (marked by arrows; green online) denote the translationally invariant states. The dark solid dots are the spurious states (see text). The dashed line denotes the yrast band, while the cusp states are marked by a circle. Energies in units of $e^2/(\kappa l_B)$. The number of translationally invariant states is much smaller than the total number of LLL states.

of the trap (for the correspondence between B and Ω , see Ref. [46]). In all studied cases [11,15,24,28,29,31,48] (including both electrons and bosons up to $N = 9$ particles), the total angular momenta of the global ground states belong to the set of magic angular momenta given by Eq. (30). We note that the emergence of these magic angular momenta are a direct signature of the molecular nature of the cusp states, a fact that further motivates our present investigations concerning the molecular description of the full LLL spectra beyond the electronic [12,13,15] cusp states.

In the LLL, all many-body wave functions have the general form [5,25,30]

$$W(z_1, z_2, \dots, z_N)|0\rangle, \quad (5)$$

where $W(z_1, z_2, \dots, z_N)$ is a homogeneous polynomial of degree L (being antisymmetric for fermions and symmetric for bosons).

In Eq. (5), the symbol $|0\rangle$ stands for a product of Gaussians [see Eq. (4)]

$$|0\rangle = \exp\left(-\sum_{i=1}^N z_i z_i^*/2\right). \quad (6)$$

To simplify the notation, this common factor will be omitted henceforth in the algebraic expressions and manipulations [except in Eqs. (18) and (33), where it is repeated for clarity]. Its contribution, however, is necessary when numerical results are calculated.

A central property of the LLL spectra is the existence of a translationally invariant (TI) subspace [5,25,30] for a given

L . This subspace is associated with a special subset of the general wave functions in Eq. (5), that is, with wave functions having TI polynomials $W(z_1, z_2, \dots, z_N)$. Specifically, the TI polynomials obey the relationship

$$W(z_1 + c, z_2 + c, \dots, z_N + c) = W(z_1, z_2, \dots, z_N), \quad (7)$$

for any arbitrary constant complex number c .

The LLL states belonging to the TI subspaces are denoted by gray solid dots (marked by an arrow; green online) in Figs. 1 and 2. The dimension $D^{\text{TI}}(L)$ of the translational invariant subspace is much smaller than the dimension $D^{\text{EXD}}(L)$ of the exact-diagonalization (EXD) [15] space (which is spanned by uncorrelated permanents or Slater determinants as discussed earlier). The remaining $D^{\text{EXD}}(L) - D^{\text{TI}}(L)$ states are *spurious* center-of-mass excitations, generated by multiplying the TI states with the operator z_c^m , $m = 1, 2, \dots$, where

$$z_c = \frac{1}{N} \sum_{i=1}^N z_i, \quad (8)$$

is the coordinate of the center of mass [49].

The energies of these spurious states coincide with those appearing at all the other smaller angular momenta [5]. Thus (see Tables I, II, and IV)

$$D^{\text{TI}}(L) = D^{\text{EXD}}(L) - D^{\text{EXD}}(L - 1). \quad (9)$$

We further note that for N particles (bosons or fermions)

$$D_b^{\text{TI}}(L) = D_f^{\text{TI}}(L + N(N - 1)/2), \quad (10)$$

where the subscripts b and f stand for bosons and fermions (electrons), respectively. $N(N - 1)/2$ is the smallest value of the total angular momentum for spin-polarized fermions in the LLL.

C. Plan of the article

The article is organized as follows. The analytic trial functions associated with pure rotations of bosonic molecules (i.e., the RBM's) are introduced in Sec. II A, followed by a description of the purely rotational electronic molecular functions (i.e., the REM's) in Sec. II B. Properties of the RBM's and REM's are discussed in Sec. II C. Section II D introduces the general rovibrational trial functions (i.e., the RVM's).

Case studies of the quantal molecular description of the LLL spectra are presented in Sec. III. In particular, Sec. III A discusses the case of $N = 3$ LLL scalar bosons, while Sec. III B discusses the case of $N = 3$ spin-polarized LLL electrons. The case of $N = 4$ LLL electrons is presented in Sec. III C, along with an analysis of the JL state (for fractional filling $\nu = 1/3$) from the viewpoint of the present molecular theory. Section III D investigates the case of $N = 5$ LLL bosons, along with an analysis of the MR state according to the molecular picture. Section IV offers a summary and discussion. Finally, the Appendix discusses the rapid-convergence properties of the RVM basis.

We note that, going from $N = 3$ to $N = 5$ particles, the molecular description requires consideration of successively larger numbers of isomeric molecular structures as elaborated in Sec. III. In particular, for $N = 3$ only one molecular isomer

is needed, while three different molecular isomers are needed for $N = 5$. It is remarkable that these isomers are independent of the statistics (bosons or fermions).

II. MOLECULAR TRIAL FUNCTIONS

The molecular trial functions introduced in this article are derived with the help of a first-principles methodology of hierarchical successive approximations that converge to the exact solution of the many-body Schrödinger equation [15]. Specifically, this methodology is based on the theory of symmetry breaking at the mean-field level and of subsequent symmetry restoration via projection techniques [15]. In this section, we present (and/or review where appropriate) this derivation in some detail.

A. Purely rotational bosonic trial functions (RBM's)

RBM analytical wave functions in the LLL for N bosons in 2D rotating traps can be derived following earlier analogous derivations for the case of electrons [12]. Our approach consists of two steps:

At the *first step*, one constructs a permanent (Slater determinant for fermions) $\Psi^N(z_1, \dots, z_N)$ out of displaced single-particle states $u(z_j, Z_j)$, $j = 1, \dots, N$ that represent scalar bosons localized at the positions Z_j , with (omitting the particle indices) $z = x + iy$ and $Z = X + iY = Re^{i\phi}$,

$$\Psi^N[z] = \text{perm}(\mathcal{M}^N[z]), \quad (11)$$

with the matrix $\mathcal{M}^N[z]$ being

$$\mathcal{M}^N[z] = \begin{bmatrix} u(z_1, Z_1) & \cdots & u(z_N, Z_1) \\ \vdots & \ddots & \vdots \\ u(z_1, Z_N) & \cdots & u(z_N, Z_N) \end{bmatrix}. \quad (12)$$

For the permanent of a matrix, we follow here the definition in Ref. [51], that is, the permanent is an analog of a determinant where all the signs in the expansion by minors are taken as positive. This definition provides an unnormalized expression for the permanent. If a normalized expression is needed, one has to multiply with a normalization constant

$$\mathcal{N} = \frac{1}{\sqrt{N! p_1! p_2! \dots p_M!}}, \quad (13)$$

where $\{p_1, p_2, \dots, p_M\}$ denote the occupations (multiplicities) of the orbitals, assuming that there are M distinct orbitals in a given permanent ($M \leq N$) [52].

In the LLL, one can specifically consider the limit when the confining potential can be neglected compared to the effect induced by the gauge field. The localized $u(z, Z)$ single-particle states (referred to also as orbitals) are then taken to be *displaced zero-node Darwin-Fock* states with appropriate Peierls phases due to the presence of a perpendicular magnetic field [see Eq. (1) in Ref. [12]] or due to the rotation of the trap with angular frequency Ω . Then, assuming a symmetric gauge, the orbitals can be represented [12,13,53] by displaced Gaussian analytic functions, centered at different positions $Z_j \equiv X_j + iY_j$ according to the equilibrium configuration of N classical point charges [54,55] arranged at the vertices

of nested regular polygons (each Gaussian representing a localized particle). Such displaced Gaussians are written as

$$u(z, Z_j) = (1/\sqrt{\pi}) \exp[-|z - Z_j|^2/2] \exp[-i(xY_j - yX_j)], \quad (14)$$

where the phase factor is due to the gauge invariance. $z \equiv x + iy$ and all lengths are in units of Λ in the case of a rotating trap or $l_B\sqrt{2}$ in the case of an applied magnetic field; see Sec. IB.

The localized orbital $u(z, Z)$ can be expanded in a series over the complete set of zero-node single-particle wave functions in Eq. (4). One gets (see Appendix in Ref. [56])

$$u(z, Z) = \sum_{l=0}^{\infty} C_l(Z) \psi_l(z), \quad (15)$$

with

$$C_l(Z) = (Z^*)^l \exp(-ZZ^*/2)/\sqrt{l!} \quad (16)$$

for $Z \neq 0$. Naturally, $C_0(0) = 1$ and $C_{l>0}(0) = 0$.

For an N -particle system, the bosons are situated at the apexes of r concentric regular polygons. The ensuing multiring structure is denoted by (n_1, n_2, \dots, n_r) with $\sum_{q=1}^r n_q = N$. The position of the j th electron on the q th ring is given by

$$Z_j^q = \tilde{Z}_q \exp[i2\pi(1-j)/n_q], \quad 1 \leq j \leq n_q. \quad (17)$$

The single permanent $\Psi^N[z]$ represents a *static* boson molecule. Using Eq. (15), one finds the following expansion (within a proportionality constant)

$$\Psi^N[z] = \sum_{l_1=0, \dots, l_N=0}^{\infty} \frac{C_{l_1}(Z_1) C_{l_2}(Z_2) \cdots C_{l_N}(Z_N)}{\sqrt{l_1! l_2! \cdots l_N!}} \times P(l_1, l_2, \dots, l_N) |0\rangle, \quad (18)$$

where $P(l_1, l_2, \dots, l_N) \equiv \text{perm}[z_1^{l_1}, z_2^{l_2}, \dots, z_N^{l_N}]$; the elements of the permanent are the functions $z_j^{l_j}$, with $z_1^{l_1}, z_2^{l_2}, \dots, z_N^{l_N}$ being the diagonal elements. The Z_k 's (with $1 \leq k \leq N$) in Eq. (18) are the Z_j^q 's of Eq. (17), but relabeled.

In Eq. (18), the common factor $|0\rangle$ represents the product of Gaussians defined in Eq. (6). To simplify the notation this common factor is usually omitted.

Second step: In the following, we will continue with the details of the complete derivation in the simplest case of a single $(0, N)$ ring. Thus we consider the special case

$$Z_j = R e^{2\pi i(1-j)/N}, \quad 1 \leq j \leq N, \quad (19)$$

where R is the radius of the single ring.

The Slater permanent $\Psi^N[z]$ breaks the rotational symmetry and thus it is not an eigenstate of the total angular momentum $\hbar\hat{L} = \hbar \sum_{j=1}^N \hat{l}_j$. However, one can restore [12,15] the rotational symmetry by applying onto $\Psi^N[z]$ the projection operator

$$\mathcal{P}_L \equiv \frac{1}{2\pi} \int_0^{2\pi} d\gamma e^{i\gamma(\hat{L}-L)}, \quad (20)$$

where $\hbar L$ are the eigenvalues of the total angular momentum.

When applied onto $\Psi^N[z]$, the projection operator \mathcal{P}_L acts as a Kronecker delta: From the unrestricted sum in Eq. (18) it picks up only those terms having a given total angular momentum L (henceforth we drop the constant prefactor \hbar when referring to angular momenta). As a result the projected wave function $\Phi_L^N = \mathcal{P}_L \Psi^N$ is written as (within a proportionality constant)

$$\Phi_L^N[z] = \sum_{l_1, \dots, l_N}^{l_1 + \dots + l_N = L} \frac{P(l_1, \dots, l_N)}{l_1! \cdots l_N!} e^{i(\phi_1 l_1 + \dots + \phi_N l_N)}, \quad (21)$$

with $\phi_j = 2\pi(j-1)/N$.

We further observe that it is advantageous to rewrite Eq. (21) by restricting the summation to the ordered arrangements $l_1 \leq l_2 \leq \dots \leq l_N$, in which case we get

$$\Phi_L^N[z] = \sum_{0 \leq l_1 \leq l_2 \leq \dots \leq l_N}^{l_1 + l_2 + \dots + l_N = L} \frac{P(l_1, \dots, l_N)}{l_1! \cdots l_N!} \times \frac{\text{perm}[e^{i\phi_1 l_1}, e^{i\phi_2 l_2}, \dots, e^{i\phi_N l_N}]}{p_1! p_2! \cdots p_M!}. \quad (22)$$

The second permanent in Eq. (22) can be shown [57] to be equal (within a proportionality constant) to a *sum* of cosine terms times a phase factor

$$e^{i\pi(N-1)L/N}, \quad (23)$$

which is independent of the individual l_j 's.

The final result for the $(0, N)$ RBM wave function is (within a proportionality constant)

$$\Phi_L^{\text{RBM}}(0, N)[z] = \sum_{0 \leq l_1 \leq l_2 \leq \dots \leq l_N}^{l_1 + l_2 + \dots + l_N = L} C_b(l_1, l_2, \dots, l_N) \times \text{perm}[z_1^{l_1}, z_2^{l_2}, \dots, z_N^{l_N}], \quad (24)$$

where the coefficients are given by different expressions for even or odd numbers of bosons N .

(i) For even N , one has

$$C_b(l_1, l_2, \dots, l_N) = \left(\prod_{i=1}^N l_i! \right)^{-1} \left(\prod_{k=1}^M p_k! \right)^{-1} \times \sum_{\sigma} \cos \left\{ [(N-1)l_{\sigma_1} + (N-3)l_{\sigma_2} + \dots + l_{\sigma_{N/2}} - l_{\sigma_{(N/2+1)}} - \dots - (N-3)l_{\sigma_{(N-1)}} - (N-1)l_{\sigma_N}] \frac{\pi}{N} \right\}, \quad (25)$$

where the summation \sum_{σ} runs over the permutations of the set of N indices $\{1, 2, \dots, N\}$.

(ii) With the notation $K = N - 1$, the corresponding coefficients for odd N are

$$C_b(l_1, l_2, \dots, l_N) = \left(\prod_{i=1}^N l_i! \right)^{-1} \left(\prod_{k=1}^M p_k! \right)^{-1} \times \sum_{\sigma\{K\}} \cos \left\{ [Kl_{\sigma_1} + (K-2)l_{\sigma_2} + \dots \right.$$

$$\left. \begin{aligned} &+ 2l_{\sigma_{(K/2)}} - 2l_{\sigma_{(K/2+1)}} - \dots \\ &- (K-2)l_{\sigma_{(K-1)}} - Kl_{\sigma_K} \end{aligned} \right\} \frac{\pi}{N}, \quad (26)$$

where $\sum_{\sigma_{\{K\}}}$ runs over all permutations of $N-1$ indices selected out from the set $\{1, 2, \dots, N\}$ (of N indices); all N selections of $N-1$ indices need to be considered.

In both Eqs. (25) and (26), the index M (with $1 \leq M \leq N$) denotes the number of different single-particle angular momenta l_j 's ($j = 1, 2, \dots, M$) in the ordered list $\{l_1, l_2, \dots, l_N\}$ and the p_k 's are the multiplicities of each one of the different l_j 's [occupations of the corresponding single-particle orbitals $\psi_{l_j}(z)$]. For example, for $N = 4$ and $\{l_1 = 2, l_2 = 2, l_3 = 2, l_4 = 5\}$, one has $M = 2$ and $p_1 = 3, p_2 = 1$; for $\{l_1 = 0, l_2 = 0, l_3 = 0, l_4 = 0\}$, one has $M = 1$ and $p_1 = 4$; for $\{l_1 = 1, l_2 = 2, l_3 = 3, l_4 = 9\}$, one has $M = 4$ and $p_1 = p_2 = p_3 = p_4 = 1$.

We further note that for both Eqs. (25) and (26) the total number of distinct cosine terms is $N!/2$ [58], with the division by 2 following from the symmetry properties of cosine, that is, from $\cos(-x) = \cos(x)$.

The RBM expression for an (n_1, n_2) two-ring configuration (with $N = n_1 + n_2$) can be derived following similar steps as in the derivation of the expressions for the multiring REM's [12]. If $L_1 + L_2 = L$, the final two-ring RBM expression is

$$\begin{aligned} &\Phi_L^{\text{RBM}}(n_1, n_2)[z] \\ &= \sum_{0 \leq l_1 \leq l_2 \leq \dots \leq l_{n_1}} \sum_{0 \leq l_{n_1+1} \leq l_{n_1+2} \leq \dots \leq l_N} C_b(l_1, l_2, \dots, l_{n_1}) \\ &\quad \times C_b(l_{n_1+1}, l_{n_1+2}, \dots, l_N) \text{perm}[z_1^{l_1}, z_2^{l_2}, \dots, z_N^{l_N}], \quad (27) \end{aligned}$$

where $C_b(l_1, l_2, \dots, l_{n_1})$ and $C_b(l_{n_1+1}, l_{n_1+2}, \dots, l_N)$ are calculated by applying the single-ring expressions of Eqs. (25) and (26).

Generalizations of expression (27) to structures with a larger number r of concentric rings involve for *each* q th ring ($1 \leq q \leq r$): (I) Consideration of a separate factor $C_b(l_{n_{q-1}+1}, l_{n_{q-1}+2}, \dots, l_{n_{q-1}+n_q})$; (II) A restriction on the summation of the associated n_q angular momenta $l_{n_{q-1}+1} + l_{n_{q-1}+2} + \dots + l_{n_{q-1}+n_q} = L_q$, with $\sum_{q=1}^r L_q = L$.

B. Purely rotational fermionic trial functions (REM's)

The REM expression for any (n_1, n_2, \dots, n_r) multiring configuration (with $N = \sum_{q=1}^r n_q$) was derived earlier in Refs. [12,13] following similar steps as those in Sec. II A. A determinant needs to be used, however, instead of a permanent to conform with the antisymmetrization properties of the electronic (fermionic) many-body wave function. If $L_1 + L_2 = L$, the final two-ring REM expression is

$$\begin{aligned} &\Phi_L^{\text{REM}}(n_1, n_2)[z] \\ &= \sum_{0 \leq l_1 < l_2 < \dots < l_{n_1} < l_{n_1+1} < \dots < l_N} C_f(l_1, l_2, \dots, l_{n_1}) \\ &\quad \times C_f(l_{n_1+1}, l_{n_1+2}, \dots, l_N) \det[z_1^{l_1}, z_2^{l_2}, \dots, z_N^{l_N}], \quad (28) \end{aligned}$$

where the fermionic coefficients $C_f(l_1, l_2, \dots, l_{n_1})$ and $C_f(l_{n_1+1}, l_{n_1+2}, \dots, l_N)$ are calculated by applying to each one of them the single-ring $[(0, N)]$ expression

$$C_f(l_1, l_2, \dots, l_N) = \left(\prod_{i=1}^N l_i! \right)^{-1} \left(\prod_{1 \leq i < j \leq N} \sin \left[\frac{\pi}{N} (l_i - l_j) \right] \right). \quad (29)$$

It is straightforward to generalize the two-ring REM expression in Eq. (28) to more complicated or simpler [i.e., $(0, N)$ and $(1, N-1)$] configurations by (I) considering a separate factor $C_f(l_{n_{q-1}+1}, l_{n_{q-1}+2}, \dots, l_{n_{q-1}+n_q})$ for each q th ring; (II) restricting the summation of the associated n_q angular momenta $l_{n_{q-1}+1} + l_{n_{q-1}+2} + \dots + l_{n_{q-1}+n_q} = L_q$, with $\sum_{q=1}^r L_q = L$.

Apart from the permanent being replaced by a determinant, we note two other main differences between the REM and RBM expressions. That is, for electrons (1) $M = N$ in all instances (single occupancy) and (2) a *product of sine* terms in the coefficients $C_f(\dots)$ replaces the *sum of cosine* terms in the coefficients $C_b(\dots)$.

C. Properties of RBM's and REM's

The analytic expressions for $\Phi_{\mathcal{L}}^{\text{RXM}}(n_1, n_2, \dots, n_r)[z]$ (the index RXM standing for either RBM or REM) describe pure molecular rotations associated with magic angular momenta

$$\mathcal{L} = \mathcal{L}_0 + \sum_{q=1}^r n_q k_q, \quad (30)$$

with k_q , $q = 1, \dots, r$ being nonnegative integers; $\mathcal{L}_0 = N(N-1)/2$ for electrons and $\mathcal{L}_0 = 0$ for bosons.

A central property of these trial functions is that identically

$$\Phi_{\mathcal{L}}^{\text{RXM}}(n_1, n_2, \dots, n_r)[z] = 0 \quad (31)$$

for both bosons and electrons when

$$\mathcal{L} \neq \mathcal{L}_0 + \sum_{q=1}^r n_q k_q. \quad (32)$$

This selection rule follows directly from the point group symmetries of the (n_1, n_2, \dots, n_r) multiring polygonal configurations. Indeed under condition (32) the $C_b(\dots)$ and $C_f(\dots)$ coefficients are identically zero, as can be easily checked using MATHEMATICA [57]. In other words, purely rotational states are allowed only for certain angular momenta that do not conflict with the intrinsic molecular point-group symmetries.

The yrast states corresponding to magic \mathcal{L} 's [Eq. (30)] are associated with the special cusp states described previously in Figs. 1 and 2 and in Sec. IB. Furthermore, the enhanced stability associated with the cusp states (see Sec. IB) is obviously due to the selection rule described by Eqs. (31) and (32).

An important property of the REM and RBM trial functions is their translational invariance (in the sense described in Sec. IB).

D. General rovibrational trial functions (RVM's)

The RVM functions that account for the general excitations of the rotating molecules have the form (within a normalization constant)

$$\Phi_{\mathcal{L}}^{\text{RXM}}(n_1, n_2, \dots, n_r) Q_{\lambda}^m |0\rangle. \quad (33)$$

The index RXM stands for either REM or RBM. The purely rotational functions $\Phi_{\mathcal{L}}^{\text{RXM}}(n_1, n_2, \dots, n_r)$ were described in detail in earlier sections. The product in Eq. (33) combines rotations with vibrational excitations, the latter being denoted by Q_{λ}^m , with λ being an angular momentum; the superscript denotes raising to a power m . Both $\Phi_{\mathcal{L}}^{\text{RXM}}$ and Q_{λ}^m are homogeneous polynomials of the complex particle coordinates z_1, z_2, \dots, z_N , of order \mathcal{L} and λm , respectively. The total angular momentum $L = \mathcal{L} + \lambda m$. Q_{λ}^m is always symmetric in these variables; $\Phi_{\mathcal{L}}^{\text{RXM}}$ is antisymmetric (symmetric) for fermions (bosons). $|0\rangle$ is the product of Gaussians defined in Eq. (6); this product of Gaussians is usually omitted.

The vibrational excitations Q_{λ} are given by the same expression for both bosons and electrons, namely, by the symmetric polynomials

$$Q_{\lambda} = \sum_{i=1}^N (z_i - z_c)^{\lambda}, \quad (34)$$

where z_c is the coordinate of the center of mass defined in Eq. (8) and $\lambda > 1$ is an integer positive number. Vibrational excitations of a similar form

$$\tilde{Q}_{\lambda} = \sum_{i=1}^N z_i^{\lambda}, \quad (35)$$

(and certain other variants) were used earlier to approximate part of the LLL spectra. Such earlier endeavors provided valuable insights, but overall they remained inconclusive; for electrons over the maximum density droplet [with magic $\mathcal{L} = \mathcal{L}_0$], see Refs. [8] and [9]; for electrons over the $\nu = 1/3$ ($\nu = \mathcal{L}_0/\mathcal{L}$) Jastrow-Laughlin trial function [with magic $\mathcal{L} = 3\mathcal{L}_0$], see Ref. [10]; and for bosons in the range $0 \leq L \leq N$, see Refs. [22,25,26].

The advantage of Q_{λ} [50] (compared to \tilde{Q}_{λ}) is that it is TI [5,25], a property shared with both $\Phi_{\mathcal{L}}^{\text{RBM}}$ and $\Phi_{\mathcal{L}}^{\text{REM}}$. In the following, we will discuss illustrative cases, which will show that the RVM functions of Eq. (33) provide a correlated basis (RVM basis) that spans the TI subspace [5,25,30] of nonspurious states in the LLL spectra.

III. MOLECULAR DESCRIPTION OF LLL SPECTRA

A. Three spinless bosons

Only the (0, 3) molecular configuration and the dipolar $\lambda = 2$ vibrations are at play (as checked numerically); the full TI spectra at any L are spanned by the wave functions

$$\Phi_{3k}^{\text{RBM}}(0, 3) Q_2^m \Rightarrow \{k, m\}, \quad (36)$$

with $k, m = 0, 1, 2, \dots$, and $L = 3k + 2m$; these states are always orthogonal.

Following Eq. (24), a simplified analytic expression for the (0,3) RBM can be derived

$$\Phi_{\mathcal{L}}^{\text{RBM}}(0, 3) = \sum_{0 \leq l_1 \leq l_2 \leq l_3}^{l_1+l_2+l_3=\mathcal{L}} C_b(l_1, l_2, l_3) \text{Perm}[z_1^{l_1}, z_2^{l_2}, z_3^{l_3}], \quad (37)$$

where the coefficients $C_b(\dots)$ are given by

$$C_b(l_1, l_2, l_3) = \left(\prod_{i=1}^3 l_i! \right)^{-1} \left(\prod_{k=1}^M p_k! \right)^{-1} \times \left\{ \sum_{1 \leq i < j \leq 3} \cos \left[\frac{2\pi(l_i - l_j)}{3} \right] \right\}, \quad (38)$$

where $1 \leq M \leq 3$ denotes the number of different single-particle angular momenta in the triad (l_1, l_2, l_3) and the p_k 's are the multiplicities of each one of these different angular momenta.

Table I provides the systematics of the molecular description for the beginning ($0 \leq L \leq 12$) of the LLL spectrum. There are several cases when the TI subspace has dimension one and the exact solution Φ^{exact} coincides with a single $\{k, m\}$ state. For $L = 0$ the exact solution coincides with $\Phi_0^{\text{RBM}} = 1$ ($Q_{\lambda}^0 = 1$); this is the only case when an LLL state has a Gross-Pitaevskii form—it is a single (normalized) permanent [see Eq. (33)] given by $|0\rangle$ as defined in Eq. (6).

For $L = 2$, we found $\Phi_{[1]}^{\text{exact}} \propto Q_2$, with the index $[i]$ indicating the energy ordering in the full EXD spectrum (including both spurious and TI states). Since [see Eq. (34)]

$$Q_2 \propto (z_1 - z_c)(z_2 - z_c) + (z_1 - z_c)(z_3 - z_c) + (z_2 - z_c)(z_3 - z_c), \quad (39)$$

this result agrees with the findings of Refs. [25,59] concerning ground states of bosons in the range $0 \leq L \leq N$.

For $L = 3$, one finds $\Phi_{[1]}^{\text{exact}} \propto \Phi_3^{\text{RBM}}$. Since [see Eq. (37)]

$$\Phi_3^{\text{RBM}} \propto (z_1 - z_c)(z_2 - z_c)(z_3 - z_c), \quad (40)$$

this result agrees again with the findings of Refs. [25,59].

For $L = 5$, the single nonspurious state is an excited one, $\Phi_{[2]}^{\text{exact}} \propto \Phi_3^{\text{RBM}} Q_2$.

For $L = 6$ ($\nu = 1/2$), the ground-state is found to be

$$\Phi_{[1]}^{\text{exact}} \propto -\frac{160}{9} \Phi_6^{\text{RBM}} + \frac{1}{4} Q_2^3 = (z_1 - z_2)^2 (z_1 - z_3)^2 (z_2 - z_3)^2, \quad (41)$$

that is, the bosonic Jastrow-Laughlin function for $\nu = 1/2$ is equivalent to an RBM state that incorporates vibrational correlations.

For $L \geq N(N-1)$ (i.e., $\nu \leq 1/2$), the EXD yrast energies equal zero and with increasing L the degeneracy of the zero-energy states for a given L increases. It is important that this nontrivial behavior is reproduced faithfully by the present method (see Table I).

B. Three electrons

Although unrecognized, the solution of the problem of three spin-polarized electrons in the LLL using molecular trial functions was presented by Laughlin in Ref. [60]. Indeed, the

TABLE I. LLL spectra of three spinless bosons interacting via a repulsive contact interaction $g\delta(z_i - z_j)$. Second column: Dimensions of the EXD and the nonspurious TI (in parentheses) spaces (the EXD space is spanned by uncorrelated permanents of Darwin-Fock orbitals). Fourth to sixth columns: Matrix elements [in units of $g/(\pi\Lambda^2)$, $\Lambda = \sqrt{\hbar/(m\omega_0)}$] of the contact interaction between the correlated RVM states $\{|k, m\rangle$ [see Eq. (36)]. The total angular momentum $L = 3k + 2m$. Last three columns: Energy eigenvalues from the RVM diagonalization of the associated matrix of dimension $D^{\text{TI}}(L)$. There is no nonspurious state with $L = 1$. The full EXD spectrum at a given L is constructed by including, in addition to the listed TI eigenvalues [$D^{\text{TI}}(L)$ in number], all the energies associated with angular momenta smaller than L . An integer in square brackets indicates the energy ordering in the full EXD spectrum (including both spurious and TI states). Seven decimal digits are displayed, but the energy eigenvalues from the RVM diagonalization agree with the corresponding EXD^{TI} ones within machine precision.

L	$D^{\text{EXD}}(D^{\text{TI}})$	$\{ k, m\rangle$	Matrix elements			Energy eigenvalues (RVM diag. or EXD ^{TI})		
0	1(1)	{0,0}	1.5000000			1.5000000[1]		
2	2(1)	{0,1}	0.7500000			0.7500000[1]		
3	3(1)	{1,0}	0.3750000			0.3750000[1]		
4	4(1)	{0,2}	0.5625000			0.5625000[2]		
5	5(1)	{1,1}	0.4687500			0.4687500[2]		
6	7(2)	{2,0}	0.0468750	0.1482318				
		{0,3}	0.1482318	0.4687500		0.0000000[1]	0.5156250[4]	
7	8(1)	{1,2}	0.4921875			0.4921875[4]		
8	10(2)	{2,1}	0.0937500	0.1960922				
		{0,4}	0.1960922	0.4101562		0.0000000	0.5039062[6]	
12	19(3)	{4,0}	7.3242187×10^{-4}	1.0863572×10^{-2}	1.5742811×10^{-2}			
		{2,3}	1.0863572×10^{-2}	0.1611328	0.2335036			
		{0,6}	1.5742811×10^{-2}	0.2335036	0.3383789	0.0000000	0.0000000	0.5002441[13]

main result of Ref. [60] [see Eq. (18) therein] was the following wave functions (we display the polynomial part only)

$$|k, m\rangle \propto \left[\frac{(z_a + iz_b)^{3k} - (z_a - iz_b)^{3k}}{2i} \right] (z_a^2 + z_b^2)^m, \quad (42)$$

where the three-particle Jacobi coordinates are

$$z_c = \frac{z_1 + z_2 + z_3}{3}, \quad (43)$$

$$z_a = \left(\frac{2}{3}\right)^{1/2} \left[\frac{z_1 + z_2}{2} - z_3 \right], \quad (44)$$

$$z_b = \frac{1}{\sqrt{2}}(z_1 - z_2). \quad (45)$$

Expression (42) is precisely of the form $\Phi_{3k}^{\text{REM}} Q_2^m$, as can be checked after transforming back to Cartesian coordinates z_1 , z_2 , and z_3 . Thus the wave functions $|k, m\rangle$ of Ref. [60] describe both pure molecular rotations as well as vibrational excitations and they cover the TI LLL subspace. We note that the pairs of indices $\{|k, m\rangle$ are universal and independent of the statistics, that is, the same for both bosons [Eq. (36)] and electrons [Eq. (42)], as can be explicitly seen through a comparison of Table I here and Table I in Ref. [60].

We further note that Laughlin did not present molecular trial functions for electrons with $N > 3$ or for bosons for any N . This is done in the present article.

C. Four electrons

For $N = 4$ spin-polarized electrons, one needs to consider two distinct molecular configurations, that is, (0, 4) and (1, 3). Vibrations with $\lambda \geq 2$ must also be considered. In this case the RVM states are not always orthogonal and the Gram-Schmidt orthogonalization is implemented.

Of particular interest is the $L = 18$ case ($\nu = 1/3$) which is considered [2] as the prototype of quantum-liquid states. However, in this case we found (see Table II) that the exact TI solutions are linear superpositions of the following seven RVM states [involving both the (0,4) and (1,3) configurations]

$$\begin{aligned} |1\rangle &= \Phi_{18}^{\text{REM}}(0, 4), & |2\rangle &= \Phi_{14}^{\text{REM}}(0, 4)Q_2^2, \\ |3\rangle &= \Phi_{10}^{\text{REM}}(0, 4)Q_2^4, & |4\rangle &= \Phi_6^{\text{REM}}(0, 4)Q_2^6, \\ |5\rangle &= \Phi_{18}^{\text{REM}}(1, 3), & |6\rangle &= \Phi_{12}^{\text{REM}}(1, 3)Q_2^3, \\ |7\rangle &= \Phi_{15}^{\text{REM}}(1, 3)Q_3. \end{aligned} \quad (46)$$

The expansion coefficients of the three lowest-in-energy EXD^{TI} states (labeled [1], [2], and [4]; see Table II) in this RVM basis are listed in Table III. One sees that for each case, one component (underlined) dominates this expansion; this applies for both the yrast state (No. [1]) and the two excitations (Nos. [2] and [4]). To further illustrate this, we display in Fig. 3 the conditional probability (pair correlation) distributions (CPD's)

$$P(z, z_0) = \langle \Phi | \sum_{i \neq j} \delta(z_i - z_0) \delta(z_j - z_0) | \Phi \rangle, \quad (47)$$

for these three EXD^{TI} states (top row) and for the RVM functions (bottom row) corresponding to the dominant expansion coefficients. The similarity of the CPD's in each column is noticeable and demonstrates that the single RVM functions capture the essence of many-body correlations in the EXD^{TI} states. Full quantitative agreement (within machine precision) in total energies can be reached by taking into consideration all seven RVM basis states [see Eq. (46)]. Naturally, a smaller number of RVM states yields intermediate degrees of high-quality quantitative agreement.

TABLE II. LLL spectra of four spin-polarized electrons interacting via the Coulomb repulsion $e^2/(\kappa|z_i - z_j|)$. Second column: Dimensions of the full EXD and the nonspurious TI (in parentheses) spaces (the EXD space is spanned by uncorrelated determinants of Darwin-Fock orbitals). Last three columns: Energy eigenvalues [in units of $e^2/(\kappa l_B)$] from the diagonalization of the Coulomb interaction in the TI subspace spanned by the trial functions $\Phi_{6+4k}^{\text{REM}}(0, 4)Q_\lambda^m$ and $\Phi_{6+3k}^{\text{REM}}(1, 3)Q_\lambda^m$ (RVM diagonalization). Third to sixth columns: The molecular configurations (n_1, n_2) and the quantum numbers k, λ , and m are indicated within brackets. There is no nonspurious state with $L = 7$. The full EXD spectrum at a given L is constructed by including, in addition to the listed TI energy eigenvalues [$D^{\text{TI}}(L)$ in number], all the energies associated with angular momenta smaller than L . An integer in square brackets indicates the energy ordering in the full EXD spectrum (including both spurious and TI states), with [1] denoting a yrast state. Eight decimal digits are displayed, but the energy eigenvalues from the RVM diagonalization agree with the corresponding EXD^{TI} ones within machine precision.

L	$D^{\text{EXD}}(D^{\text{TI}})$	$[(n_1, n_2)\{k, \lambda, m\}]$	Energy eigenvalues (RVM diag. or EXD ^{TI})		
6	1(1)	[(0,4){0,λ,0}]	2.22725097[1]		
8	2(1)	[(0,4){0,2,1}]	2.09240211[1]		
9	3(1)	[(1,3){1,λ,0}]	1.93480798[1]		
10	5(2)	[(0,4){1,λ,0}] [(0,4){0,2,2}]	1.78508849[1]	1.97809256[3]	
11	6(1)	[(1,3){1,2,1}]	1.86157215[2]		
12	9(3)	[(0,4){1,2,1}] [(0,4){0,2,3}] [(1,3){2,λ,0}]	1.68518201[1]	1.76757420[2]	1.88068652[5]
13	11(2)	[(1,3){1,2,2}] [(0,4){1,3,1}]	1.64156849[1]	1.79962234[5]	
14	15(4)	[(0,4){2,λ,0}] [(0,4){1,2,2}] [(0,4){0,2,4}] [(1,3){2,2,1}]	1.50065835[1]	1.63572496[2]	1.72910626[5]
15	18(3)	[(1,3){3,λ,0}] [(1,3){2,3,1}] [(1,3){1,3,2}]	1.52704695[2]	1.62342533[3]	1.74810279[8]
18	34(7)	[(0,4){3,λ,0}] [(0,4){2,2,2}] [(0,4){1,2,4}] [(0,4){0,2,6}] [(1,3){4,λ,0}] [(1,3){2,2,3}] [(1,3){3,3,1}]	1.30572905[1]	1.41507954[2]	1.43427543[4]
			1.50366728[8]	1.56527615[11]	1.63564655[15]
			1.68994048[20]		

The celebrated Jastrow-Laughlin ansatz [2],

$$\Phi^{\text{JL}}[z] = \prod_{1 \leq i < j \leq N} (z_i - z_j)^{2p+1}, \quad (48)$$

was given exclusively an interpretation of a quantum-fluid state [2,11]. However, since the RVM functions span the TI subspace, it follows that any TI trial function (including the JL ansatz and the compact CF states) can be expanded in the RVM basis. As an example, we give in Table III (fourth column) the RVM expansion of the JL state for $N = 4e$ and $L = 18$. One sees that, compared to the EXD yrast state (first column), the relative weight of the pure (0,4) REM (denoted by |1>) is reduced, while the weights of higher-in-energy vibrational excitations are enhanced. In this context, the liquid characteristics are due to the stronger weight of molecular vibrations that diminish the rigidity of the molecule.

Of great interest also is the $L = 30$ ($\nu = 1/5$) case, which in the composite-fermion picture was found to be susceptible

TABLE III. $N = 4$ LLL electrons with $L = 18$: Expansion coefficients in the RVM basis (labeled by the $|i\rangle$'s) for the three lowest-in-energy EXD^{TI} states (labeled [1], [2], [4]; see Table II). The fourth column gives the RVM expansion coefficients of the corresponding Jastrow-Laughlin expression.

RVM	EXD ^{TI} [1]	EXD ^{TI} [2]	EXD ^{TI} [4]	JL
1>	<u>0.9294</u>	-0.3430	0.0903	0.8403
2>	-0.1188	-0.0693	<u>0.8930</u>	-0.1086
3>	0.0067	0.0382	-0.2596	0.0076
4>	0.0137	0.0191	-0.0968	0.0395
5>	0.2540	<u>0.8486</u>	0.1519	0.4029
6>	0.0211	0.0283	0.3097	0.0616
7>	-0.2387	-0.3935	0.0877	-0.3380

to a competition [17] between crystalline and liquid orders. However, we found that the exact nonspurious states for $L = 30$ are actually linear superpositions of the following 19 [= $D^{\text{TI}}(L = 30)$] RVM functions

$$\begin{aligned} &\Phi_{6+4k}^{\text{REM}}(0, 4)Q_2^{12-2k}, \quad \text{with } k = 0, 1, 2, 3, 4, 5, 6; \\ &\Phi_{6+3k}^{\text{REM}}(1, 3)Q_2^{12-3k/2}, \quad \text{with } k = 2, 4, 6; \\ &\Phi_{6+4k}^{\text{REM}}(0, 4)Q_3^{8-4k/3}, \quad \text{with } k = 0, 3; \\ &\Phi_{6+3k}^{\text{REM}}(1, 3)Q_3^{8-k}, \quad \text{with } k = 2, 3, 4, 5, 6, 7, 8. \end{aligned} \quad (49)$$

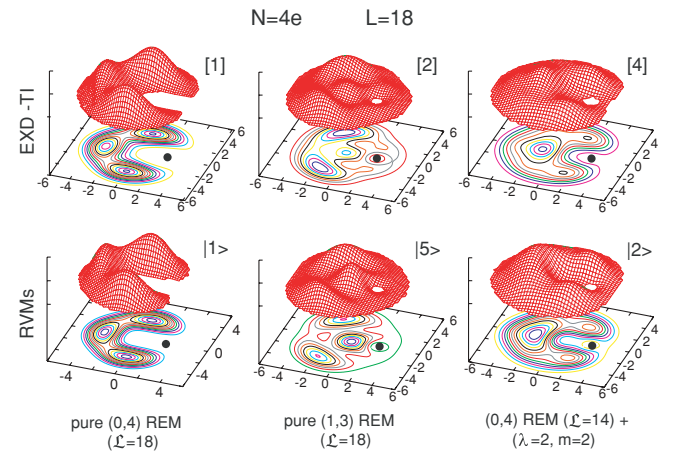


FIG. 3. (Color online) CPDs for $N = 4$ LLL electrons with $L = 18$ ($\nu = 1/3$). Top row: The three lowest-in-energy EXD^{TI} states (see Table II). Bottom row: The RVM trial functions associated with the largest expansion coefficients (underlined, see Table III) of these three EXD^{TI} states in the correlated RVM basis. See the text for details. The solid dot denotes the fixed point \mathbf{r}_0 . Distances in nm.

TABLE IV. LLL spectra of five spinless bosons interacting via a repulsive contact interaction $g\delta(z_i - z_j)$. Second column: Dimensions of the full EXD and the nonspurious TI (in parentheses) spaces (the EXD space is spanned by uncorrelated permanents of Darwin-Fock orbitals). Last three columns: Energy eigenvalues [in units of $g/(\pi\Lambda^2)$] from the diagonalization of the contact interaction in the TI subspace spanned by the trial functions $\Phi_{5k}^{\text{RBM}}(0, 5)Q_\lambda^m$, $\Phi_{4k}^{\text{RBM}}(1, 4)Q_\lambda^m$, and $\Phi_{3k}^{\text{RBM}}(2, 3)Q_\lambda^m$ (RVM diagonalization). Third to sixth columns: The molecular configurations (n_1, n_2) and the quantum numbers k, λ , and m are indicated within brackets. There is no nonspurious state with $L = 1$. The full EXD spectrum at a given L is constructed by including, in addition to the listed TI energy eigenvalues [$D^{\text{TI}}(L)$ in number], all the energies associated with angular momenta smaller than L . An integer in square brackets indicates the energy ordering in the full EXD spectrum [including both spurious and TI states (EXD^{TI})], with [1] denoting an yrast state. Eight decimal digits are displayed, but the energy eigenvalues from the RVM diagonalization agree with the corresponding EXD^{TI} ones within machine precision.

L	$D^{\text{EXD}}(D^{\text{TI}})$	$[(n_1, n_2)\{k, \lambda, m\}]$	Energy eigenvalues (RVM diag. or EXD ^{TI})		
0	1(1)	[(0,5){0,λ,0}]	5.00000000[1]		
2	2(1)	[(0,5){0,2,1}]	3.75000000[1]		
3	3(1)	[(0,5){0,3,1}]	3.12500000[1]		
4	5(2)	[(1,4){1,λ,0}] [(0,5){0,2,2}]	2.50000000[1]	3.18750000[3]	
5	7(2)	[(0,5){1,λ,0}] [(0,5){0,5,1}]	1.87500000[1]	3.03125000[3]	
6	10(3)	[(1,4){1,2,1}] [(0,5){0,2,3}] [(0,5){0,3,2}]	1.90664171[2]	2.42925914[3]	3.02347415[5]
7	13(3)	[(1,4){1,3,1}] [(0,5){1,2,1}] [(2,3){1,2,2}]	1.77354877[1]	2.07258062[4]	3.00543311[7]
8	18(5)	[(1,4){2,λ,0}] [(1,4){1,2,2}] [(0,5){1,3,1}] [(0,5){0,2,4}] [(2,3){2,2,1}]	1.18821986[1]	1.60795253[2]	1.91688009[6]
9	23(5)	[(1,4){1,5,1}] [(0,5){1,2,2}] [(2,3){3,λ,0}] [(2,3){2,3,1}] [(2,3){1,3,2}]	2.24905854[8]	3.00273273[11]	
10	30(7)	[(0,5){2,λ,0}] [(0,5){1,5,1}] [(0,5){0,5,2}] [(1,4){2,2,1}] [(1,4){1,2,3}] [(1,4){1,3,2}] [(2,3){2,2,2}]	1.12895814[1]	1.52195553[3]	1.89102917[7]
11	37(7)	[(0,5){1,3,2}] [(0,5){1,2,3}] [(1,4){2,3,1}] [(2,3){3,2,1}] [(2,3){2,5,1}] [(2,3){1,2,4}] [(2,3){1,4,2}]	2.06074601[10]	3.00082677[15]	
12	47(10)	[(0,5){2,2,1}] [(1,4){3,λ,0}] [(1,4){2,2,2}] [(1,4){2,4,1}] [(1,4){1,4,2}] [(1,4){1,2,4}] [(2,3){4,λ,0}] [(2,3){3,3,1}] [(2,3){1,3,3}] [(2,3){0,4,3}]	0.90026059[1]	1.29362646[4]	1.51398054[5]
			1.66194766[8]	1.95923264[14]	2.12274862[17]
			3.00035191[21]		
			1.03755324[2]	1.07552423[3]	1.50429489[7]
			1.58737738[10]	1.94750687[18]	2.03365831[20]
			0.61480761[1]	0.93028069[3]	1.05066256[5]
			1.34022509[10]	1.50000444[11]	1.50755634[13]
			1.64279523[18]	1.98164620[27]	2.05477689[29]
			3.00004768[36]		

Diagonalization of the Coulomb interaction in this TI subspace yielded an energy $0.25084902 e^2/(\kappa l_B)$ per electron for the yrast state; this value agrees again, within machine precision, with the EXD result. The most sophisticated variants of the composite-fermion theory [including composite-fermion diagonalization (CFD), composite-fermion crystal (CFC), and mixed liquid-CFC states [11,17–19]] fall short in this respect. Indeed the following higher energies were found [17]: 0.250863(6) (CFD), 0.25094(4) (mixed), 0.25101(4) (CFC); numbers shown in parentheses are statistical uncertainties arising from Monte Carlo sampling. The CFD basis is not TI [18,19]. Consequently, to achieve machine-precision accuracy, the CFD will have to be performed in the larger space of dimension $D^{\text{EXD}}(L = 30) = 169$.

D. Five bosons

For $N = 5$ spinless bosons, one needs to consider rovibrational states [see Eq. (33)] for *three* distinct molecular configurations, $\Phi_{5k}^{\text{RBM}}(0, 5)Q_\lambda^m$, $\Phi_{4k}^{\text{RBM}}(1, 4)Q_\lambda^m$, and $\Phi_{3k}^{\text{RBM}}(2, 3)Q_\lambda^m$. Vibrations with $\lambda \geq 2$ must also be considered; since the RVM states are not always orthogonal, a Gram-Schmidt orthogonalization is implemented. Table IV summarizes the quantal molecular description in the start of the LLL spectrum ($0 \leq L \leq 12$).

Of particular interest is the $L = 8$ case, since it corresponds to the bosonic MR state, given [24,31] by the analytic

expression

$$\Phi^{\text{MR}}[z] = \mathcal{S} \prod_{i < j \in A} (z_i - z_j)^2 \prod_{k \in l \in B} (z_k - z_l)^2, \quad (50)$$

where sets A and B contain $(N - 1)/2$ and $(N + 1)/2$ particles, respectively, if N is odd. (For N even, both sets contain $N/2$ particles.) \mathcal{S} symmetrizes over all possible ways of carrying such a division of N particles into the two sets.

Based on sizable overlaps with the EXD wave functions [24,31], the bosonic MR states [7] are thought to represent the yrast states in the LLL with the same angular momentum, $L = (N - 1)^2/2$ for odd N and $L = N(N - 2)/2$ for even N [24].

However, for $N = 5$ and $L = 8$, we found (see Table IV) that the exact TI solutions are linear superpositions of the following *five* RVM states [involving both the (0,5), (1,4), and (2,3) configurations]

$$\begin{aligned} |1\rangle &= \Phi_8^{\text{RBM}}(1, 4), & |2\rangle &= \Phi_4^{\text{RBM}}(1, 4)Q_2^2, \\ |3\rangle &= \Phi_5^{\text{RBM}}(0, 5)Q_3, & |4\rangle &= \Phi_0^{\text{RBM}}(0, 5)Q_2^4, \\ |5\rangle &= \Phi_6^{\text{RBM}}(2, 3)Q_2. \end{aligned} \quad (51)$$

The expansion coefficients of the yrast EXD^{TI} state (labeled [1]; see Table IV) in this RVM basis are listed in Table V. One sees that one component (labeled |1), underlined) dominates this expansion. To further illustrate this, we display in Fig. 4

TABLE V. $N = 5$ LLL bosons with $L = 8$: Expansion coefficients in the RVM basis [Eq. (51)] (labeled by the $|i\rangle$'s). The second column gives the yrast EXD^{TI} state (labeled [1]; see Table IV). The third column gives the RVM expansion coefficients of the corresponding MR expression [Eq. (50)].

RVM	EXD ^{TI} [1]	MOORE-READ
1⟩	<u>0.7879</u>	-0.5159
2⟩	-0.1162	0.1502
3⟩	-0.6005	<u>0.7999</u>
4⟩	-0.0684	0.1873
5⟩	-0.0198	-0.1908

the N -body correlation functions for this EXD^{TI} state (i.e., the quantity)

$$P(z; z_1^0, z_2^0, z_3^0, z_4^0) \propto |\Phi(z; z_1^0, z_2^0, z_3^0, z_4^0)|^2, \quad (52)$$

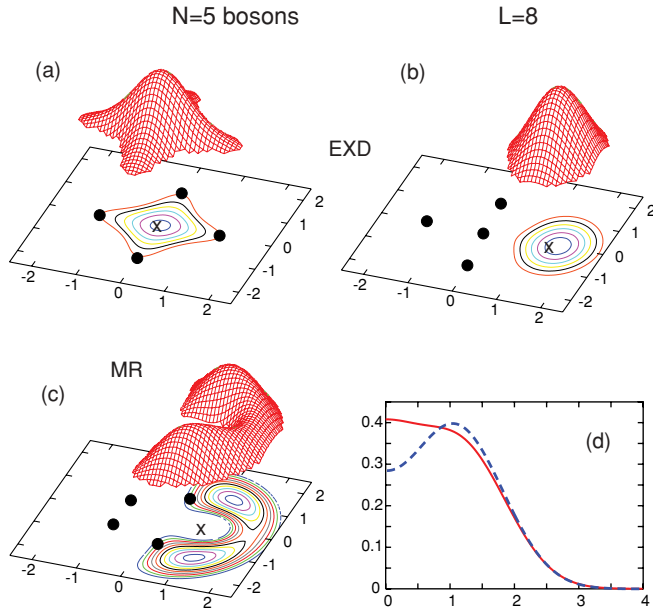


FIG. 4. (Color online) N -body correlation functions for $N = 5$ LLL bosons with total angular momentum $L = 8$. (a-b): The yrast EXD^{TI} state (labeled [1]; see Table IV). (c): The MR state given by Eq. (50). (d): Corresponding radial single-particle densities for the yrast EXD^{TI} state (solid line; red online) and the MR state (dashed line; blue online). Solid dots denote the four fixed points placed at $r_0 \exp[j\pi i/2]$, $j = 1, 2, 3, 4$ (with $r_0 = 1.3\Lambda$) in (a), $(0, 0)$ and $r_0 \exp[j\pi i/2]$, $j = 1, 2, 3$ (with $r_0 = 1.3\Lambda$) in (b), and $r_0 \exp[2j\pi i/5]$, $j = 1, 2, 3, 4$ (with $r_0 = 1.02\Lambda$) in (c). Crosses denote the expected position of the fifth localized boson according to the classical (1,4) polygonal-ring configuration in (a-b) and the (0,5) single-ring configuration in (c). For the (1,4) configuration, there are two nonequivalent ways of choosing the four fixed points. In (c), a node, associated with an octupole vibration (see text), develops at the expected position of the fifth particle. In the radial single-particle densities in (d), note the maximum (local minimum) at the origin of the solid line (dashed line) in agreement with the underlying (1,4)[(0,5)] configuration.

which gives the probability distribution of finding the fifth boson at a position z under the condition that the remaining four bosons are fixed at positions z_j^0 , $j = 1, 2, 3, 4$. The N -body correlations exhibit a (1,4) configuration that corresponds to the dominant $\Phi_8^{\text{RBM}}(1, 4)$ RVM component [component |1], defined in Eq. (51)]. In particular, when the four fixed points are forming a complete square inscribed in a circle of radius $r_0 = 1.3\Lambda$ [see Fig. 4(a)], the fifth boson is localized around the origin. When three fixed points coincide with only three vertices of this square, with the fourth being at the origin, the fifth boson is localized around the fourth vertex of the square, as expected from the classical (1,4) configuration.

In contrast to this, we found that the MR state [see Eq. (50)] exhibits a drastically different behavior in its N -body correlation function [portrayed in Fig. 4(c)]. To analyze this behavior, we expanded the MR state (for $N = 5$ bosons and $L = 8$) in the RVM basis of Eq. (51). As was the case with the JL 1/3 function for $N = 4$ electrons, such an expansion is possible due to the fact that the MR state is TI. The corresponding expansion coefficients are listed in Table V. It is remarkable that one dominant coefficient (underlined) does appear, but it is associated with the RVM basis state $\Phi_5^{\text{RBM}}(0, 5)Q_3$ (denoted as |3⟩), instead of the RVM state |1⟩ that dominates the expansion of the EXD^{TI} yrast state. This basis state |3⟩ corresponds to an octupolar single-phonon vibration of a (0,5) polygonal configuration, and this is reflected in the N -body correlation plotted in Fig. 4(c). Indeed, with the four fixed points positioned at the vertices of a regular pentagon inscribed in a circle of radius $r_0 = 1.02\Lambda$, the probability of finding the remaining boson is concentrated in the neighborhood of the fifth vertex that completes the pentagon (denoted by X), but in addition it exhibits a prominent node precisely at X.

Figure 4(d) contrasts the radial single-particle densities of the EXD^{TI} and MR states. Naturally, the radial single-particle densities provide a reduced amount of information regarding the correlation structure. However, note that they reflect the underlying (1,4) and (0,5) molecular configurations through the maximum at the origin of the solid line (EXD^{TI} state) or the local minimum at the origin of the dashed line (MR state), respectively.

This analysis cautions against drawing conclusions by relying exclusively on overlaps (as is often the practice in the literature of fast rotating ultracold bosons [24,31]). Indeed, we can conclude that the MR state examined here disagrees in an essential way with the EXD many-body wave functions.

TABLE VI. Matrix elements of the contact interaction [in units of $g/(\pi\Lambda^2)$] between the RVM basis states for $N = 5$ LLL bosons with $L = 8$. The notation for the RVM functions is the same as in Eq. (51). Only four decimal points are shown.

	1⟩	2⟩	3⟩	4⟩	5⟩
1⟩	1.3964	1.5813×10^{-2}	0.2567	7.7995×10^{-2}	0.1358
2⟩		2.4933	-0.1896	-0.2631	-0.3711
3⟩			1.5554	0.0000	0.1930
4⟩				2.4609	0.2492
5⟩					2.0588

TABLE VII. RVM-diagonalization total energies [in units of $g/(\pi\Lambda^2)$], relative errors, and overlaps at each intermediate step for the case of the yrast state for $N = 5$ LLL bosons with $L = 8$ (see Sec. III D). The notation for the RVM functions is the same as in Eq. (51). The composition of each step is shown in the second column. The last row displays the corresponding quantities for the MR function [Eq. (50)].

Step	Composition	Energy	Relative error (%)	Overlap
1	$ 1\rangle$	1.3964006(RVM)	17.5	0.788
2	$ 1\rangle + 3\rangle$	1.2071388(RVM)	1.6	0.990
3	$ 1\rangle + 3\rangle + 2\rangle$	1.1947104(RVM)	0.500	0.997
4	$ 1\rangle + 3\rangle + 2\rangle + 4\rangle$	1.1884821(RVM)	0.02	0.9998
5	$ 1\rangle + 3\rangle + 2\rangle + 4\rangle + 5\rangle$	1.1882199(RVM)	0.00	1.000
	MOORE-READ	1.2658991	6.5	0.913

We stress that the EXD yrast states with the same angular momenta as the MR states exhibit correlations that conform with the molecular structures associated with the magic angular momenta defined in Eq. (30). In particular, $L = 8$ (corresponding to the MR state for $N = 5$) is a magic angular momentum associated with a (1,4) configuration (i.e., $8 \bmod 4 = 0$). Another example is $L = 12$ (corresponding to the MR state for $N = 6$). In this latter case, the EXD N -body correlation function for the yrast state was studied in Ref. [29], where it was found (see in particular Figs. 5 and 6 therein) that it conformed to a (0,6) polygonal-ring configuration, in agreement with the fact that $12 \bmod 6 = 0$.

IV. SUMMARY AND DISCUSSION

The many-body Hilbert space corresponding to the TI part of the LLL spectra of small systems (whether fermions or bosons and for both low and high angular momenta) is spanned by the RVM trial functions introduced in Eq. (33). The yrast and excited states for both short and long-range interactions can always be expressed as linear superpositions of these RVM functions. Thus the nature of strong correlations in the LLL reflects the emergence of intrinsic point-group symmetries associated with rotations and vibrations of molecules formed through particle localization. We stress the validity of the molecular theory for *low* angular momenta, where “quantum-liquid” physical pictures [2,11,31] were thought to apply exclusively. Our analysis suggests that liquid-type pictures, associated with TI trial functions (e.g., the Jastrow-Laughlin,

compact composite-fermion, and MR functions) are reducible to a description in terms of an excited rotating or vibrating quantal molecule.

In addition to these conceptual advances, from a computational point of view, the introduction of the RVM correlated basis is promising concerning future computational developments. Indeed, it has the potential for enabling controlled and stepwise improvements of the variational wave function, in analogy with previous experiences from correlated bases in other fields of many-body physics [39–41]. Such developments may enhance computational capabilities for systems with a larger number of particles than it is currently possible.

The main body of the present article consisted of two parts. The general theoretical background of our methodology was presented in Sec. II, while Sec. III was devoted to case studies. In particular:

The analytic trial functions associated with pure rotations of bosonic molecules (i.e., the RBM’s) were derived in Sec. II A, followed by a description of the purely rotational electronic molecular functions (i.e., the REM’s) in Sect. II B. Properties of the RBM’s and REM’s and their association with magic angular momenta were discussed in Sec. II C, and the general rovibrational trial functions (i.e., the RVM’s) were introduced in Sec. II D.

Concerning illustrative examples of the quantal molecular description of the LLL spectra, Sec. III A discussed the case of $N = 3$ LLL scalar bosons, while Sec. III B investigated the case of $N = 3$ spin-polarized LLL electrons. The case

TABLE VIII. RVM-diagonalization total energies [in units of $e^2/(\kappa l_B)$], relative errors, and overlaps at each intermediate step for the case of the yrast state for $N = 4$ LLL electrons with $L = 18$ (see Sec. III C). The notation for the RVM functions is the same as in Eq. (46). The composition of each step is shown in the second column. The last row displays the corresponding quantities for the Laughlin function [Eq. (48)].

Step	Composition	Energy	Relative error (%)	Overlap
1	$ 1\rangle$	1.3217670(RVM)	1.23	0.929
2	$ 1\rangle + 5\rangle$	1.3174550(RVM)	0.90	0.961
3	$ 1\rangle + 5\rangle + 7\rangle$	1.3081859(RVM)	0.19	0.992
4	$ 1\rangle + 5\rangle + 7\rangle + 2\rangle$	1.3059258(RVM)	0.015	0.99965
5	$ 1\rangle + 5\rangle + 7\rangle + 2\rangle + 6\rangle$	1.3058052(RVM)	0.006	0.99988
6	$ 1\rangle + 5\rangle + 7\rangle + 2\rangle + 6\rangle + 4\rangle$	1.3057413(RVM)	0.001	0.99997
7	$ 1\rangle + 5\rangle + 7\rangle + 2\rangle + 6\rangle + 4\rangle + 3\rangle$	1.3057290(RVM)	0.000	1.00000
	JASTROW-LAUGHLIN	1.3105953	0.37	0.979

of $N = 4$ LLL electrons was elaborated in Sec. III C, along with an analysis of the Jastrow-Laughlin state (for fractional filling $\nu = 1/3$) from the viewpoint of the present molecular theory. Finally, Sec. III D studied the case of $N = 5$ LLL bosons, along with an analysis of the MR state according to the molecular picture. It was shown that the intrinsic correlation structure of the MR state disagrees strongly with that of the EXD wave function [in spite of having a rather good overlap with the EXD state, calculated by us to be 0.913 (see also Ref. [24])].

The Appendix discusses in detail the rapid-convergence properties of the RVM basis.

In the case of bosons in harmonic traps, mean-field vortex solutions of the Gross-Pitaevskii (GP) equation have been proven most useful for the interpretation of experiments in a variety of situations of Bose-Einstein condensates with very large N ; see, e.g., Refs. [61,62]. Consequently, the results presented in this article and previously [15,28,29] pertaining to crystalline-type correlations in finite systems with a small number N of LLL bosons (as well as the earlier prediction of the development of molecular-crystalline patterns in nonrotating finite boson systems [63]) are unexpected. While these results are of intrinsic interest for small systems, one may also inquire about the size-dependent evolution of the properties of the system with increasing N . This question, and in particular the possibility of a transition of LLL bosons to mean-field GP behavior for large N , is of high importance conceptually and practically and we expect that it will be the focus of future experimental and theoretical studies [64].

ACKNOWLEDGMENTS

This work was supported by the US Department of Energy (DOE) (FG05-86ER45234).

APPENDIX: CONVERGENCE IN THE RVM BASIS

1. The example of $N = 5$ bosons

In this section, we analyze in detail the convergence properties of the RVM diagonalization for the yrast state of $N = 5$ bosons with $L = 8$ (a case associated with a MR function) that was discussed in Sec. III D.

In Table VI, we display the coupling matrix elements for the contact interaction between the RVM basis functions given in Eq. (51). The convergence properties in the RVM basis cannot be immediately seen from an inspection of these coupling

matrix elements; while most of the off-diagonal elements in Table VI are smaller than the differences between the associated diagonal elements, a couple of them are indeed larger.

The fast-convergence properties of the RVM basis can be seen through a tabulation of the intermediate RVM-diagonalization total energies as the size of the RVM basis increases in successive steps. In Table VII, in addition to these intermediate RVM energies, we also display the corresponding relative error (relative to the EXD result) and the corresponding overlap with the EXD wave function for the yrast state (denoted by the index [1] in Sec. III D).

We stress that convergence (as a function of the number of the RVM basis functions used in the calculation) is seen from Table VII to be achieved rapidly (i.e., already with the use of only two basis functions one obtains a relative error of 1.6% for the energy eigenvalue and a 99% overlap with the exact eigenfunction). In particular, we note that at the second step the RVM wavefunction is already more accurate compared to the MR function, which exhibits a relative error of 6.5% for the energy and an overlap of 91.3% [see Table VIII].

2. The example of $N = 4$ electrons

In this section, we analyze in detail the convergence properties of the RVM diagonalization for the yrast state of $N = 4$ electrons with $L = 18$ (a case associated with a Jastrow-Laughlin function) that was discussed in Sec. III C.

As previously, the convergence properties of the RVM basis can be seen through a tabulation of the intermediate RVM-diagonalization total energies as the size of the RVM basis increases in successive steps. In Table VIII, in addition to these intermediate RVM energies, we also display the corresponding relative error (relative to the EXD result) and the corresponding overlap with the EXD wave function for the yrast state (denoted by the index [1] in Sec. III C).

Convergence (as a function of the number of the RVM basis functions used in the calculation) is seen from Table VIII to be achieved rapidly (i.e., already with the use of only two basis functions one obtains a relative error of 0.90% for the energy eigenvalue and a 99% overlap with the exact eigenfunction). In particular, we note that at the third step the RVM wave function is already more accurate compared to the Laughlin function: Indeed the latter exhibits a relative error of 0.37% for the energy and an overlap of 97.9%, compared to 0.19% and 99.2%, respectively, in the case of the former [see Table VIII].

[1] D. C. Tsui, H. L. Stormer, and A. C. Gossard, *Phys. Rev. Lett.* **48**, 1559 (1982).
 [2] R. B. Laughlin, *Phys. Rev. Lett.* **50**, 1395 (1983); *Rev. Mod. Phys.* **71**, 863 (1999), and references therein.
 [3] F. D. M. Haldane, *Phys. Rev. Lett.* **51**, 605 (1983).
 [4] B. I. Halperin, *Phys. Rev. Lett.* **52**, 1583 (1984).
 [5] S. A. Trugman and S. Kivelson, *Phys. Rev. B* **31**, 5280 (1985).

[6] J. K. Jain, *Phys. Rev. Lett.* **63**, 199 (1989).
 [7] G. Moore and N. Read, *Nucl. Phys.* **B360**, 362 (1991).
 [8] M. Stone, H. W. Wyld, and R. L. Schult, *Phys. Rev. B* **45**, 14156 (1992).
 [9] J. H. Oaknin, L. Martín-Moreno, J. J. Palacios, and C. Tejedor, *Phys. Rev. Lett.* **74**, 5120 (1995).
 [10] J. J. Palacios and A. H. MacDonald, *Phys. Rev. Lett.* **76**, 118 (1996).

- [11] J. K. Jain, *Composite Fermions* (Cambridge University Press, Cambridge, England, 2007), and references therein.
- [12] C. Yannouleas and U. Landman, Phys. Rev. B **66**, 115315 (2002).
- [13] C. Yannouleas and U. Landman, Phys. Rev. B **68**, 035326 (2003).
- [14] C. Yannouleas and U. Landman, Phys. Rev. B **70**, 235319 (2004).
- [15] C. Yannouleas and U. Landman, Rep. Prog. Phys. **70**, 2067 (2007).
- [16] C. C. Chang, G. S. Jeon, and J. K. Jain, Phys. Rev. Lett. **94**, 016809 (2005).
- [17] C. C. Chang, C. Töke, G. S. Jeon, and J. K. Jain, Phys. Rev. B **73**, 155323 (2006).
- [18] G. S. Jeon, C. C. Chang, and J. K. Jain, Phys. Rev. B **69**, 241304(R) (2004).
- [19] G. S. Jeon, C. C. Chang, and J. K. Jain, Eur. Phys. J. B **55**, 271 (2007).
- [20] B. Wunsch, T. Stauber, and F. Guinea, Phys. Rev. B **77**, 035316 (2008).
- [21] I. Romanovsky, C. Yannouleas, and U. Landman, Phys. Rev. B **79**, 075311 (2009).
- [22] B. R. Mottelson, Phys. Rev. Lett. **83**, 2695 (1999).
- [23] N. R. Cooper and N. K. Wilkin, Phys. Rev. B **60**, R16279 (1999).
- [24] N. K. Wilkin and J. M. F. Gunn, Phys. Rev. Lett. **84**, 6 (2000).
- [25] Th. Papenbrock and G. F. Bertsch, Phys. Rev. A **63**, 023616 (2001).
- [26] M. Ueda and T. Nakajima, Phys. Rev. A **64**, 063609 (2001).
- [27] M. Popp, B. Paredes, and J. I. Cirac, Phys. Rev. A **70**, 053612 (2004).
- [28] N. Barberán, M. Lewenstein, K. Osterloh, and D. Dagnino, Phys. Rev. A **73**, 063623 (2006).
- [29] L. O. Baksmaty, C. Yannouleas, and U. Landman, Phys. Rev. A **75**, 023620 (2007).
- [30] S. Viefers, J. Phys. Condens. Matter **20**, 123202 (2008).
- [31] N. R. Cooper, Adv. Phys. **57**, 539 (2008), and references therein.
- [32] E. Sarajlic, N. Gemelke, S.-W. Chiow, S. Herrman, H. Müller, and S. Chu, in *Pushing the frontiers of atomic physics: Proceedings of the XXI International Conference on Atomic Physics*, edited by R. Côté, Ph.L. Gould, M. Rozman, and W. W. Smith (World Scientific, Hackensack, New Jersey, USA, 2009), p. 34.
- [33] S. K. Baur, K. R. A. Hazzard, and E. J. Mueller, Phys. Rev. A **78**, 061608(R) (2008).
- [34] M. I. Parke, N. K. Wilkin, J. M. F. Gunn, and A. Bourne, Phys. Rev. Lett. **101**, 110401 (2008).
- [35] A. Bourne, J. M. F. Gunn, and N. K. Wilkin, Phys. Rev. A **76**, 053602 (2007).
- [36] A yrast state has the lowest energy at a given L .
- [37] *Classical* approaches have also been used for constructing molecular models of the *lower part* of the LLL spectra. They perform better at high L (with $\nu < 1/9$); see P. A. Maksym, Phys. Rev. B **53**, 10871 (1996); J.-P. Nikkarila and M. Manninen, Solid State Commun. **141**, 209 (2007). As stressed in Ref. [56] and in Ch. 7.3 of Ref. [15], such classical molecular analogs correspond to highly *floppy* rotors with an L -dependent, variable moment of inertia. This allows for ground states with nonvanishing angular momenta in agreement with the EXD LLL yrast bands portrayed in Figs. 1 and 2. *Rigid* rotors with an L -independent moment of inertia (associated with an $L = 0$ ground state and an yrast band $\propto L^2$) were found for electrons in quantum dots only at zero magnetic fields, [see, e.g., C. Yannouleas and U. Landman, Phys. Rev. Lett. **85**, 1726 (2000); Phys. Rev. B **69**, 113306 (2004); L. Zeng, W. Geist, W. Y. Ruan, C. J. Umrigar, and M. Y. Chou, Phys. Rev. B **79**, 235334 (2009)].
- [38] Ref. [5] multiplied the elementary symmetric polynomials by a Pauli-exclusion single-determinant factor to generate a basis spanning the fermionic TI subspace, but which has no physical picture associated with it.
- [39] J. W. Clark and E. Feenberg, Phys. Rev. **113**, 388 (1959).
- [40] J. W. Clark and P. Westhaus, Phys. Rev. **141**, 833 (1966).
- [41] H. Müther and A. Polls, Prog. Part. Nucl. Phys. **45**, 243 (2000), in particular Sec. 2.4.
- [42] G. S. Jeon, C. C. Chang, and J. K. Jain, J. Phys. Condens. Matter **16**, L271 (2004).
- [43] Note that the CF basis and corresponding CF diagonalization have been formulated only for the case of electrons in the LLL. To date, the application of the CF methodology to LLL bosons (see, e.g., Refs. [23,31]) is limited to the simpler mean-field picture (see p. L276 of Ref. [42]), which omits residual two-body interactions.
- [44] The lack of translational invariance in the CF basis can be seen from the fact that for certain pairs, $(L, L + 1)$, of adjacent angular momenta the CF diagonalization yields states with the same energy. In this case, the $L + 1$ CF state is trivially a center-of-mass excitation of the L CF state. For $N = 4e$, such pairs of degenerate CF states are endemic in Table I of Ref. [19]; for example, $L = 10$ and $L = 11$ have the same V_{CF} energy of $1.7849 e^2/\kappa l_B$, $L = 14$ and $L = 15$ have the same V_{CF} energy of $1.501 e^2/\kappa l_B$, and so on. Similar $(L, L + 1)$ pairs of degenerate CF states are also prominent in the CF yrast energies in all other cases with $N > 4$ presented in Ref. [19]. On the contrary, such pairs are missing from Table II in this article, which summarizes the energies according to the RVM diagonalization.
- [45] T. L. Ho, Phys. Rev. Lett. **87**, 060403 (2001).
- [46] We note the correspondence $\omega_c \rightarrow 2\Omega$ (see also Ref. [29]).
- [47] In the quantum Hall effect literature, the cusp states are commonly described as incompressible since excitation from each of the corresponding global ground states to the corresponding lowest excited state entails an energy gap due to the enhanced stability.
- [48] J. K. Jain and T. Kawamura, Europhys. Lett. **29**, 321 (1995).
- [49] Although TI, the Hamiltonian in Eq. (3) does not separate the center-of-mass coordinate z_c from the internal ones. Such a separation is always possible if the external potential confinement is harmonic and this extends also in the presence of a magnetic field (or fast rotation) even when the external potential confinement can be neglected [the case of the Hamiltonian in Eq. (3)]. For the case of $N = 3e$ electrons in the LLL, this separation was carried out explicitly in Ref. [60] via the introduction of appropriate Jacobi coordinates [see Eqs. (43), (44), and (45)]. In this case, only the TI spectrum was involved (consisting of the eigenenergies of the internal Hamiltonian). Due to this separability, the general wave-function solution associated with the Hamiltonian in Eq. (3) can be written as
- $$\propto z_c^{L_c} \exp(-z_c^* z_c/2) \Phi^{\text{internal}} [z_2^J, \dots, z_N^J],$$
- where z_i^J , $i = 2, \dots, N$ denote the internal Jacobi coordinates. Multiplication of this expression by z_c raises the value of the center-of-mass angular momentum L_c by unity (from L_c to $L_c + 1$), without modifying the energy of the original state due

- to the absence of an external confining potential. This accounts for the spurious degenerate energies (dark solid dots) in Figs. 1 and 2.
- [50] For bosons, Ref. [25] studied some aspects of the Q_λ excitations in the range $0 \leq L \leq N$.
- [51] E. W. Weisstein, *Permanent*. From *MathWorld*—<http://mathworld.wolfram.com/Permanent.html>.
- [52] For another mathematically different (but equivalent) definition of a normalized permanent, see Eq. (A1) in Ref. [29].
- [53] K. Maki and X. Zotos, *Phys. Rev. B* **28**, 4349 (1983).
- [54] Yu. E. Lozovik, *Usp. Fiz. Nauk* **153**, 356 (1987) [*Sov. Phys. Usp.* **30**, 912 (1987)].
- [55] V. M. Bedanov and F. M. Peeters, *Phys. Rev. B* **49**, 2667 (1994); M. Kong, B. Partoens, and F. M. Peeters, *Phys. Rev. E* **65**, 046602 (2002).
- [56] Y. Li, C. Yannouleas, and U. Landman, *Phys. Rev. B* **73**, 075301 (2006).
- [57] Most of the algebraic manipulations reported here were performed using MATHEMATICA; see S. Wolfram, *Mathematica: A System for Doing Mathematics by Computer* (Addison-Wesley, Reading, MA, 1991).
- [58] E. W. Weisstein, *Permutation*. From *MathWorld*—<http://mathworld.wolfram.com/Permutation.html>. See also <http://en.wikipedia.org/wiki/Permutation> (in *Wikipedia*).
- [59] R. A. Smith and N. K. Wilkin, *Phys. Rev. A* **62**, 061602(R) (2000).
- [60] R. B. Laughlin, *Phys. Rev. B* **27**, 3383 (1983).
- [61] F. Dalfovo, S. Giorgini, L. Pitaevskii, and S. Stringari, *Rev. Mod. Phys.* **71**, 463 (1999); G. Baym, *J. Low Temp. Phys.* **138**, 601 (2005).
- [62] A. L. Fetter, *Rev. Mod. Phys.* **81**, 647 (2009).
- [63] I. Romanovsky, C. Yannouleas, and U. Landman, *Phys. Rev. Lett.* **93**, 230405 (2004).
- [64] In the case of 2D electrons under high magnetic field (in the LLL), it is known that many-body correlated behavior (fractional quantum Hall effect) maintains (and thus requires theoretical treatment beyond the mean field) as $N \rightarrow \infty$. In this context, the question of a transition of LLL bosons to mean-field GP behavior for large N is a challenging open topic of current research. Among some of the possible scenarios, we note the “heavy-center-of-mass” proposal for the yrast states with low angular momenta ($0 \leq L \leq N$) in Sec. 2.3.1 of Ref. [31] and the time-dependent vortex-nucleation-through-a-turbulent-phase suggestion in D. Dagnino, N. Barberan, M. Lewenstein, and J. Dalibard, *Nat. Phys.* **5**, 431 (2009). A recent mathematically rigorous study; [E. H. Lieb, R. Seiringer, and J. Yngvason, *Phys. Rev. A* **79**, 063626 (2009)] concerning upper and lower variational bounds finds that the exact yrast energy associated with the bosonic global Hamiltonian [see Eq. (2)] coincides for *large* N and *small* L with that of the mean-field Gross-Pitaevskii approach under the condition $g \ll N\omega$, where $\omega = \omega_0 - \Omega$ is the *difference* between the trapping frequency and the rotational frequency. For the interaction-only LLL Hamiltonian [see Eq. (3)], one effectively has $\omega = 0$ and the condition $g \ll N\omega$ seems to preclude the emergence of GP behavior in any region of the interaction-only LLL spectra considered in this article, except in the trivial case of a noninteracting gas (when $g = 0$). Further theoretical investigations are needed to clarify these issues.